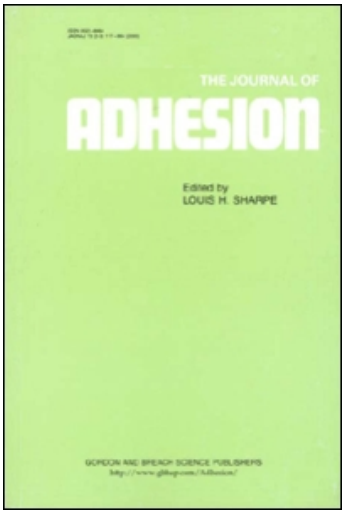

The Journal of Adhesion
Publication details, including instructions for authors and subscription information:
http://www.informaworld.com/smpp/title~content=t713453635

Adhesion and Debonding of Soft Elastic Films on Rough and Patterned Surfaces

Jayati Sarkar[a]; Ashutosh Sharma[a]; Vijay Shenoy[b]
[a] Department of Chemical Engineering, Indian Institute of Technology, Kanpur, India [b] Material Research Centre, Indian Institute of Science, Bangalore, India

To cite this Article Sarkar, Jayati , Sharma, Ashutosh and Shenoy, Vijay(2005) 'Adhesion and Debonding of Soft Elastic Films on Rough and Patterned Surfaces', The Journal of Adhesion, 81: 3, 271 — 295
To link to this Article: DOI: 10.1080/00218460590944558
URL: http://dx.doi.org/10.1080/00218460590944558

The Journal of Adhesion, 81:271–295, 2005

ISSN: 0021-8464 print/1545-5823 online
DOI: 10.1080/00218460590944558

Taylor & Francis
Taylor & Francis Group

Adhesion and Debonding of Soft Elastic Films on Rough and Patterned Surfaces

Jayati Sarkar
Ashutosh Sharma
Department of Chemical Engineering, Indian Institute of Technology, Kanpur, India

Vijay Shenoy
Material Research Centre, Indian Institute of Science, Bangalore, India

With the help of simulations based on energy minimization, we have studied the effect of roughness of a rigid contactor with sinusoidal and step patterns on the adhesion-debonding cycle of a soft thin elastic film. The surface instability engendered by attractive forces between the contactor and the film produces a regularly spaced array of columns in the bonding phase. The inter-column spacing is governed largely by periodicity of the contactor pattern. Decreased periodicity of the pattern favors intermittent collapse of columns rather than a continuous peeling of contact zones. An increase in the amplitude of roughness decreases the maximum force required for debonding and increases the snap-off distance. The net effect results in a reduced work for debonding. Introduction of noise and increased step-size in simulations decreases the pull-off force and the snap-off distance, as in the case of a smooth contactor. Finally the study reveals that a patterned contactor can be used as a potential template in the patterning of soft interfaces.

Keywords: Elastic film; Interfacial crack; Adhesion; Debonding; Patterning

Received 23 September 2004; in final form 6 December 2004.

This paper is one of a collection of articles honoring Manoj Chaudhury, the recipient in February 2005 of *The Adhesion Society Award for Excellence in Adhesion Science, Sponsored by 3M*.

We are pleased to be a part of the *Festschrift* for Manoj K. Chaudhury, who initiated us in the area of elastomer adhesion and whose work has been an inspiration for us. Discussions with Anand Jagota and Animangsu Ghatak are gratefully acknowledged. We also thank the nanosciences program of the Department of Science and Technology, Government of India for supporting this work.

Address correspondence to Ashutosh Sharma, Department of Chemical Engineering, Indian Institute of Technology, Kanpur 208016, India. E-mail: ashutos@iitk.ac.in

INTRODUCTION

Adhesion-debonding cycle or tack test of pressure sensitive adhesives (PSA) [1–8] has attracted much attention because it gives a direct measure of the pull-off force and the strength of the adhesive joints. The failure in such PSA, with pronounced viscoelastic effects, has been studied to understand the roles of random cavities or defects [7] and sites of surface roughness [8]. Most studies have considered the film surface, rather than the contactor surface, to be rough and usually consisting of randomly distributed spherical asperities [9–12]. These studies have addressed the behavior of contact area and contact pressure for these rough elastic film surfaces [9–10], as well as the time evolution of contact in viscoelastic materials [11–12]. Additionally, the surface roughness of the punch or the contactor also plays an important role in the adhesion-debonding cycle by decreasing the pull-off force and a simultaneous increase of strain [13].

Very recent studies of adhesion-debonding on purely incompressible elastic films with smooth flat surfaces [14–15] reveal spontaneous formation of nano-cavities and bridges during contact at the soft-interfaces, even without any surface roughness or pre-existing defects. The surface instability engenders a regular pattern at a uniform spacing of about $3h$, where h is the thicknesses of such soft elastic films. These non-random patterns arising from contact instabilities in purely elastic films are either in the form of labyrinth structures or equi-spaced fingers [16–20]. Theoretical studies [21–24] reveal that the instabilities in these films get triggered by the intersurface van der Waals or other attractive forces when the separation distance between the contacting surfaces reaches a critical distance ($d_c < 10\,\text{nm}$). The elastic forces in the film play a stabilizing role. This leads to the formation of patterns with wavelengths in linear proportion to the film thickness and unaffected by the nature and potential of the interactions. The surface instability of elastic films without any mass transport is different from the roughening of solid films by surface diffusion [25–28] and also different from the instability of thin viscous liquid films, where the wavelength depends strongly on the intermolecular potential [29–32].

Recent studies [14–15] on adhesion-debonding of purely elastic films interacting with a smooth contactor have addressed several issues regarding the patterns and forces during an adhesion-debonding cycle, including the metastable pathways of debonding and understanding of pull-off forces that are orders of magnitude less than that required to separate two flat surfaces. Using the same formalism [14–15], we study here the effects of roughness of contactor

on the patterns, forces, and mechanism of debonding on an initially smooth film devoid of any pre-existing asperities or surface roughness. We also address the issue of whether a periodically rough contactor with a lithographically engineered pattern (~10 nm amplitude) can be used as a template for patterning of soft elastic films.

The amplitude of contactor roughness considered here is of the order of 10 nm, which is characteristic of materials considered to be rather "smooth" such as unpolished silicon wafer, glass, plastic, and quartz with which controlled experiments are usually performed. It may be noted that the contactor roughness is still large compared to the range of intersurface interactions such as the van der Waals force considered here. The effect of higher amplitude roughness (few microns) may be felt only for very thick and softer films where debonding distances are very large. However, higher contactor roughness for the films considered here presents no new features because the contact zones are localized near the protruding tip of the contactor, regardless of its roughness once it is more than some critical value. Thus, the influence of amplitude of roughness becomes progressively smaller as the amplitude increases.

MODEL

Figure 1 denotes the schematic diagram of a soft, thin, elastic film under the influence of a patterned rough contactor. The contactor under consideration has step or sinusoidal profile with an amplitude a_p and wavelength λ_p as shown in the figure. The mean surface of the contactor is at a distance d from the undeformed surface of the flat film. The profile of the patterned contactor at lateral coordinate x_1 is denoted by v^p (x_1, d). The incompressible elastic film is of thickness h and μ is the shear modulus. When the effective gap distance between the protruded area of the rough contactor and the surface of the film declines below a critical distance d_c ($\sim 10\,nm$), the van der Waals and other attractive forces between the surfaces become destabilizing and engender deformation in the film as shown schematically by the broken lines in Figure 1. If v^f denotes the displacement vector of the elastic film, the surface deformation of the film normal to the free surface can be represented by:

$$v_2^{\mathrm{f}}(\mathrm{x}_1, 0) = \sum_{n=0}^{N-1} a_n \cos(\mathrm{k_n x_1}) \tag{1}$$

where a_n is the nth Fourier coefficient and k_n ($= 2\pi n/L_1$, L_1 being the length of the film along x_1 direction) is the wave-number of this mode.

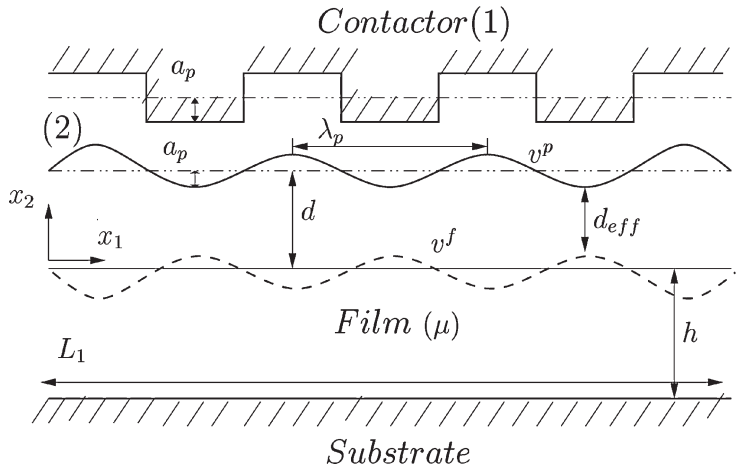

FIGURE 1 Schematic diagram of a soft thin incompressible elastic film of length L_1, thickness h and shear modulus μ rigidly bonded to the substrate at one end and under the influence of a patterned contactor with (1) step and (2) sinusoidal profile of amplitude a_p and wavelength λ_p, at the other end with a mean-surface to surface separation distance of d. A Cartesian coordinate system (x_1–x_2) is used for the analysis. The surface deformation of the film is denoted by v^f and the profile of the patterned contactor by v^p such that the effective gap-distance at any point is given by $d_{eff} = d + v^p(x_1, d) - v_2{}^f(x_1, 0)$.

In this 2-D analysis, the length of the film along the direction perpendicular to the (x_1–x_2) plane is considered to be much larger than the other two directions to assume plane strain considerations.

The interaction potential is dependant on the effective gap distance d_{eff} $(= d + v^p(x_1,\ d) - v_2{}^f(x_1,\ 0))$ between the contactor and the film surface. The interaction considered consists of a long range van der Waals attraction and a shorter range repulsion.

$$U(d_{eff}) = -\frac{A}{12\pi d_{eff}^2} + \frac{B}{d_{eff}^4} \tag{2}$$

where A is the Hamaker constant and B is the coefficient of repulsion set from the conditions: (a) The excess force (per unit area) is zero at the equilibrium separation distance (d_e), ($U'(d_e) = 0$) and is repulsive at closer distances, (b) the interaction potential at the equilibrium separation distance is equivalent to the adhesive energy at contact, or $U(d_e) = \Delta G$. The adhesion-debonding characteristics depend largely on the adhesive energy (ΔG) and the stiffness of the force at

equilibrium, rather than on the detailed form of the potential and its decay behavior [15]. In the simulations reported here, $\Delta G = 10.6\,\mathrm{mJ/m^2}$ and $A = 10^{-20}$ J were chosen.

The deformation caused by the attractive force is counteracted by the stored elasticity in the incompressible film

$$\Pi_E = \int_V \frac{1}{2}\sigma_{ij}\varepsilon_{ij}dV \tag{3}$$

where $\boldsymbol{\varepsilon} = \nabla \boldsymbol{v}^f + \nabla^{\mathrm{T}}\boldsymbol{v}^f$ is the strain and $\boldsymbol{\sigma} = \mu(\nabla \boldsymbol{v}^f + \nabla^{\mathrm{T}}\boldsymbol{v}^f) + p\boldsymbol{I}$ is the stress developed in the film. The equilibrium displacement field that develops in the film satisfies the rigid boundary condition of zero displacement at the film substrate interface $\boldsymbol{v}^f(x_1,-h) = 0$, zero shear stress condition at the surface $\sigma_{ij}(x_1,\ 0) = 0$ and stress equilibrium condition $\nabla\cdot\boldsymbol{\sigma} = 0$ at the bulk. The displacement field evaluated from the resulting differential equations gives the normal stresses in the film as [14, 15, 23]:

$$\sigma_{22}(x_1,0) = 2\mu\sum_{n=0}^{N-1} a_n k_n \frac{\left(1+\cosh(2k_nh)+2(k_nh)^2\right)}{(\sinh(2k_nh)-2k_nh)}\cos(k_nx_1) \tag{4}$$

and the elastic energy as:

$$\Pi_E = \pi\mu\frac{L_1}{2}\sum_{n=0}^{N-1} n a_n^2 k_n \frac{\left(1+\cosh(2k_nh)+2(k_nh)^2\right)}{(\sinh(2k_nh)-2k_nh)} \tag{5}$$

(A detail derivation of equations (4) and (5) is available in [23]).

Thus the total energy in terms of the Fourier coefficients is given by

$$\Pi = \pi\mu\frac{L_1}{2}\sum_{n=0}^{N-1} n a_n^2 k_n \frac{\left(1+\cosh(2k_nh)+2(k_nh)^2\right)}{(\sinh(2k_nh)-2k_nh)} + \int_0^{L_1} U\left(\sum_{n=0}^{N-1} d + v^p(x_1,d) - a_n\cos(k_nx_1)\right)dx_1 \tag{6}$$

where $U(d + v^p - v_2^f)$ above denotes the interaction energy as a function of local separation distance. For a smooth contactor, minimization of the above total energy with respect to Fourier amplitudes (a_n) gives the condition $Y = \sigma_{22}/v_2$, where $Y = (\partial^2 U/\partial d^2)$ is the stiffness of the interaction force evaluated at the mean intersurface distance. The wavenumber of instability at its onset [21–23], $kh = 2.12$ ($\lambda \sim 3\,h$), is obtained by minimization of Y with respect to kh, which also gives the condition for the onset of instability as $Yh/\mu > 6.2$ [21–23]. Thus,

for a flat contactor, the surface instability produces columns with the mean spacing of about $3h$ [14–15]. However, as shown later, the lengthscale of instability (column spacing) for a rough contactor is determined largely by the periodicity of roughness, at least in the range investigated here ($\lambda_p \sim h$ to 10 h).

A conjugate gradient scheme was employed to search the Fourier coefficients (a_n) that give the minimum energy at a given separation distance. Equation 1 thus gives the stable equilibrium profile of the film at a given position of the contactor. In our simulations, the equilibrium solution obtained by energy minimization was verified additionally by calculating the stresses, which show that the elastic stress indeed equals the adhesive force per unit area at every point on the surface of the film. The local stability of the structure was confirmed by reconvergence to the equilibrium solution after it is perturbed slightly. To realize the adhesion-debonding cycle in simulations, the intersurface distance is first reduced until the onset of surface instability (column formation), when the effective gap-distance $d_{eff} = d_c$ and then withdrawn in the step-size of s. The optimal Fourier coefficients obtained at each step become the initial guesses for the energy minimization search initiated at the next step of withdrawal. In experiments, small scale defects, high frequency roughness and other external mechanical noise and disturbances are also often present. To incorporate these effects in the simulations, the optimized Fourier coefficients obtained from one step are multiplied by $(1 + r)$, where r is a random number between $-\varepsilon$ and ε, before proceeding to the next step of withdrawal. The next section details the film morphologies thus obtained by the simulations at each stage of debonding.

MORPHOLOGIES AND MODES OF FAILURES INVOLVED IN THE ADHESION-DEBONDING CYCLES

When the effective gap distance between the rough contactor and the film surface is below a critical separation distance d_c, the van der Waals attractive force become effective and engenders instability at the film surface. Since the effective gap distance between the patterned contactor and the film surface is lowest at the protruded tips of the contactor, these are the regions where the instability first initiates as shown in Figure 2(A) for a film with $h = 0.1\,\mu$m, $\mu = 0.1$ Mpa, $\Delta G = 10.6\,\text{mJ/m}^2$ and $A = 10^{-20}$ J and a critical separation distance of 4 nm. The film surface spontaneously transforms into columns that bridge the gap between the film and the tips of the contactor. As the sinusoidal contactor ($a_p = 20$ nm, $\lambda_p = 6.4$ h) is withdrawn at step-sizes

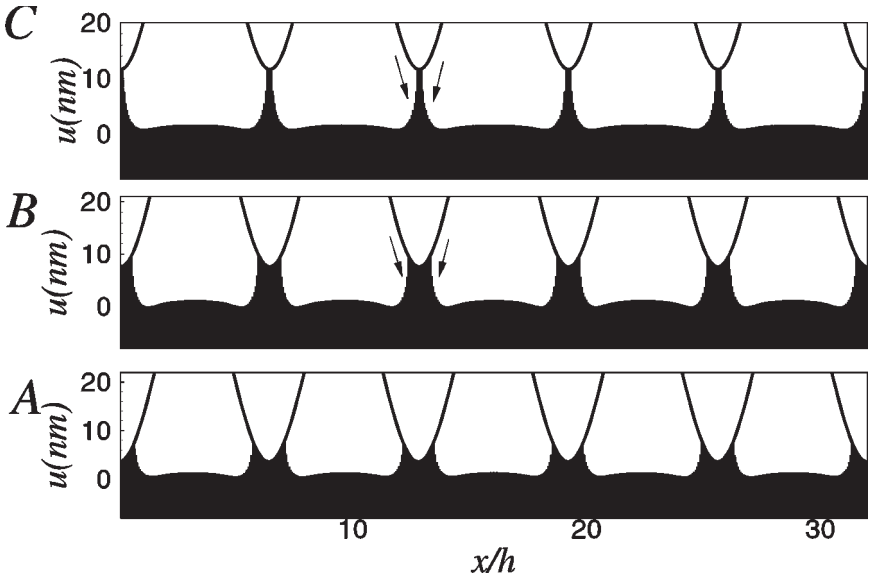

FIGURE 2 The peeling mode of debonding for a film with $h = 0.1\,\mu\text{m}$, $\mu = 0.1\,\text{MPa}$, $A = 10^{-20}\text{J}$, $\Delta G = 10.6\,\text{mJ/m}^2$ under the influence of a sinusoidal contactor of $a_p = 20\,\text{nm}$ and $\lambda_p = 6.4\,\text{h}$. The critical separation distance is 4 nm and the contactor is withdrawn at a step-size of 2 nm. The columns peel from the sides of the contactor tip as indicated by the arrows.

of 2 nm up to a distance d_{max} the columns remain *pinned* to the contactor and simply get stretched without any change in their contact area. The thickness of the film at the base of the intervening cavities declines concurrently (not shown in the figure). On further withdrawal, the columns recede sideways by *peeling* from the surface of the protruded areas of the contactor as indicated by the arrows in Figure 2(B) and at later stages, the film clings only to the tips of the contactor as indicated in Figure 2(C). The contact area that the film makes with the patterned contactor thereby decreases on withdrawal and at snap-off the film completely loses contact (debonding).

In many experiments, the withdrawal or debonding phase is not initiated at d_c (where the film first makes adhesive contact), but the contactor is first brought into more intimate contact with the film by further reducing the distance ($< d_c$) before starting the debonding phase [1–3, 8, 13]. In this study, we have also carried our simulations by bringing the contactor to a distance where $d_{eff} \sim 1\,\text{nm}$ before initiating the debonding phase. Figure 3 depicts how the contact area between a sinusoidal contactor and the film changes with separation

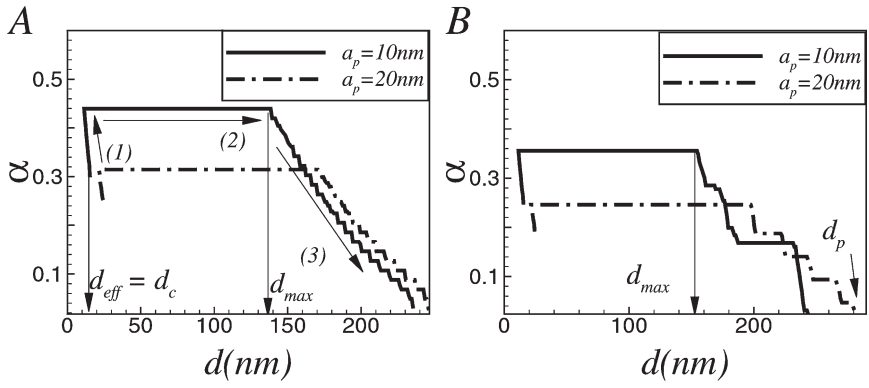

FIGURE 3 Variation of the fractional contact area with separation distance from intimate contact for a film with $h = 1.0\,\mu m$ under the influence of a sinusoidal contactor of wavelengths (A) $\lambda_p = 6.4\,h$ and (B) $\lambda_p = 1.45\,h$. All other parameters are same as in Figure 2. In the bonding region when the effective separation distance is below $d_c(\sim 7.6\,nm)$ (1) the contact area increases. In the pinning region of debonding (2) the contact area remains constant. In the third region (3) the contact area decreases either uniformly marking the peeling mode of debonding as in (A) or in steps as in (B) marking the column collapse mode of failure.

distance when debonding is initiated from intimate contact (film of thickness $h = 1\,\mu m$, $\mu = 0.1\,MPa$ and $A = 10^{-20}\,J$). Figure 3(A) represents the case when the wavelength of the patterned contactors (λ_p) is 6.4 h and amplitudes of roughness (a_p) are 10 nm and 20 nm respectively. The contact area increases when the contactor plate is brought to contact below d_c. This is the bonding phase indicated by the arrow (1) in the figure. The contactor plate is then withdrawn marking the debonding phase. For distances below d_{max} the contact area remains constant marking the *pinning phase* of withdrawal (marked by arrow (2)). Beyond this distance, the contact area decreases smoothly marking the "peeling mode" (marked by arrow (3)). It is evident that there is a hysteresis present between the bonding and debonding phases. The contact area during debonding at d_c is higher than that when the contact plate if first brought to contact at d_c. The figure also reveals that as the amplitude of roughness increases, the area of contact with the film is less. The reason behind this is apparent from Figures 4(A) and (B) which present magnified views of a single column in contact with patterned contactors of 10 nm and 20 nm amplitudes of roughness respectively. Although a higher amplitude rough surface has a higher surface area compared to lower amplitude rough surface or a flat

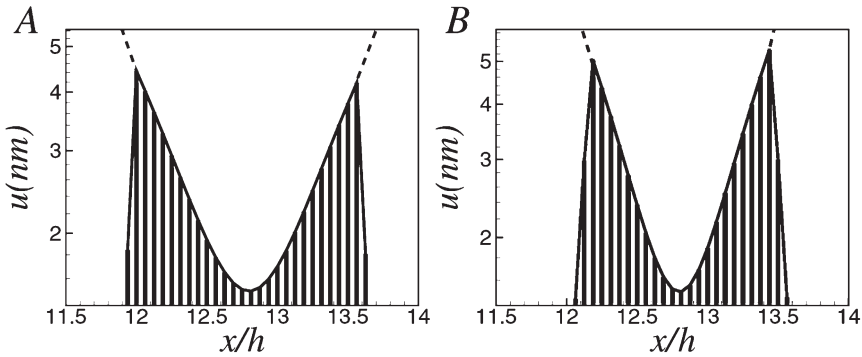

FIGURE 4 Magnified view of a single column as shown in Figure 2(A) for amplitude of roughness of the sinusoidal contactor 10 nm for (A) and 20 nm for (B). The contactor is marked by the broken line of the figure. The distance separating the film and the contactor is the equilibrium separation distance d_e(= 0.1117 nm) everywhere.

surface, the columns do not cover the whole surface of the rough contactor, but cover only the tips as shown in the figures. Thus, for a higher amplitude rough surface, the effective part of the protruded area in contact with the film is less than that of lower amplitude rough surfaces.

When periodicity (λ_p) of the patterned contactor is lower, it induces larger number (per unit length of film) of slender and more stressed columns. In such cases, (for example, $\lambda_p = 1.45\,\mathrm{h}$ in Fig. 3B) it can be seen that the contact area after d_{max} does not decrease smoothly due to continuous peeling, but does so in steps. This stepwise decrease in contact area occurs because some of the columns in contact snap back during withdrawal while the others remain in contact. So in addition to the peeling mode, the decrease in the number of columns also account for the changes in the contact area. This mode of failure is reminiscent of the *intermittent column collapse mode* for a flat contactor [14–15] where introduction of noise effectively imparts roughness to the system.

The critical minimum distance at the onset of instability is nearly independent of the roughness; for example ($\mu = 0.1\,\mathrm{MPa}$, $h = 0.1\,\mu\mathrm{m}$), $d_c \sim 4\,\mathrm{nm}$ and $\sim 3.7\mathrm{nm}$, respectively for two sinusoidal contactors characterized by $a_p = 10\,\mathrm{nm}$, $\lambda_p = 6.4\,\mathrm{h}$ and $a_p = 20\,\mathrm{nm}$, $\lambda_p = 1.45\,\mathrm{h}$.

The wavelength of the instability (λ) nearly replicates the periodicity of the patterned contactor (λ_p), both for higher and lower amplitude of roughness, until final snap-off occurs as shown in Figure 5(A). For lower λ_p of the pattern, the wavelength of the film

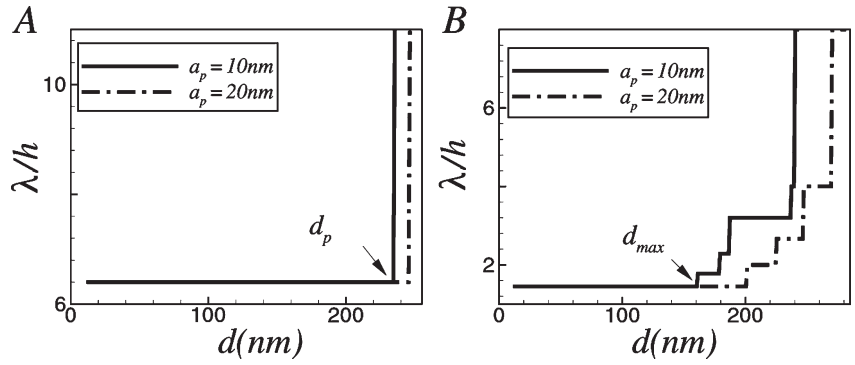

FIGURE 5 Variation of the wavelength of the evolving morphologies starting from intimate contact for a film as in Figure 3 and a sinusoidal contactor of wavelength (A) $\lambda_p = 6.4\,\mathrm{h}$ and (B) $\lambda_p = 1.45\,\mathrm{h}$. In (A) $\lambda \sim \lambda_p$ up to snap-off and in (B) $\lambda \sim \lambda_p$ up to d_{max} after which it increases.

resembles those of the patterned contactor ($\lambda \approx \lambda_p = 1.45\,\mathrm{h}$) until d_{max} after which the wavelength goes on increasing in steps as the spacing between the columns increase because of detachment of some of the columns. This feature is present both for higher and lower amplitude of roughness as shown in Figure 5(B).

The discussion thus far concerns the contactors that have smoothly varying sinusoidal profiles. For contactors with sharper features such as a step-like protrusion, the morphologies that develop are shown in Figure 6. At a critical separation distance, the columns form and cover completely only the protruded areas (Fig. 6(A)). When the contactor plate is withdrawn, the peeling mode of debonding is observed by which the contact area of the columns decrease sideways as marked by the arrows in the figure. The uniform decrease of contact area after d_{max} during withdrawal from intimate contact for $\lambda_p = 6.4\,\mathrm{h}$ is shown in Figure 7(A) for both 10 nm and 20 nm amplitude of roughness. Figure 7(B) shows that the contact area decreases in step-wise fashion for lower periodicity rough contactors ($\lambda_p = 1.45\,\mathrm{h}$), similar to the case of the sinusoidal contactors signifying column collapse mode of failure (both for amplitude of roughness 10 nm and 20 nm). There is however two marked differences in the failure modes obtained from sinusoidal and step-profile contactors, both arising for the same reasons. For the step profile contactor, it can be seen in Figures 7(A) and (B) that there is no bonding and debonding hysteresis, in contrast to the case of sinusoidal contactors. Moreover, the differences in the morphologies are not significant for the step contactors having different amplitudes

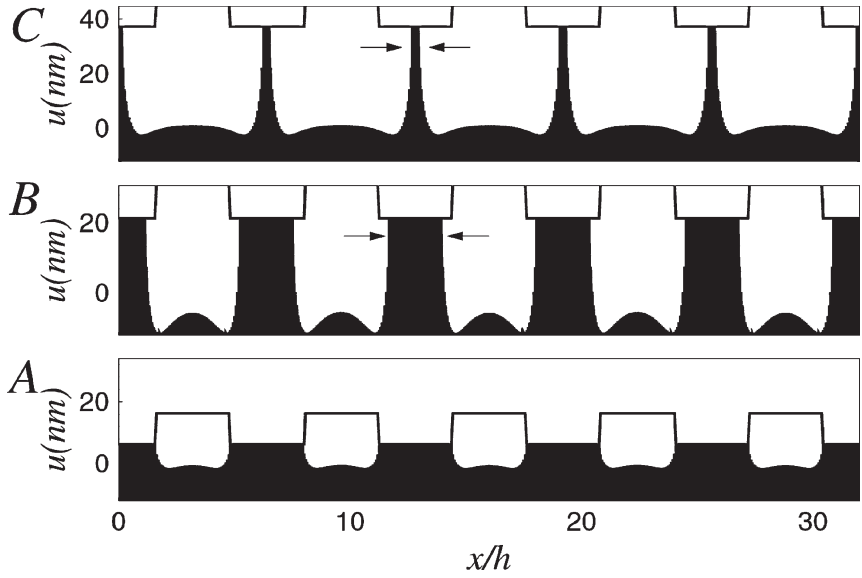

FIGURE 6 The peeling mode debonding as indicated by the arrows for a film with $h = 1\,\mu m$, $\mu = 0.1\,MPa$, $A = 10^{-20}J$ and a step profile contactor of $a_p = 10\,nm$ and $\lambda_p = 6.4\,h$ when withdrawn from d_c ($\sim$7.6 nm) at a step-size of 1 nm.

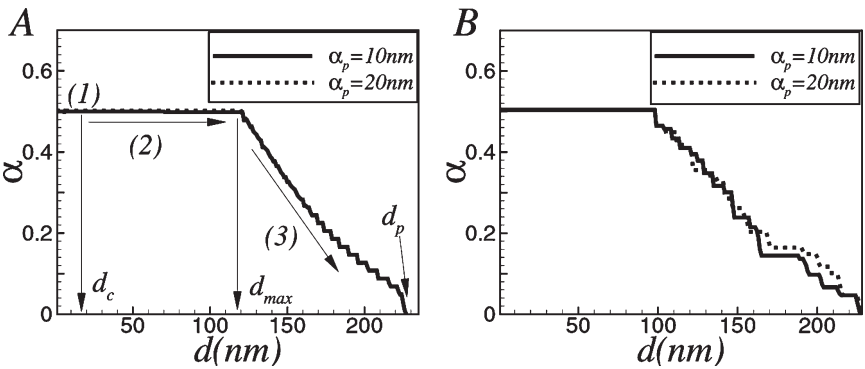

FIGURE 7 Variation of the fractional contact area with separation distance starting from intimate contact for a film as in Figure 6 and a step contactor of wavelength (A) $\lambda_p = 6.4\,h$ and (B) $\lambda_p = 1.45\,h$. During bonding phase (1) the contact area remains constant (no hysteresis). During debonding, in the pinning region (2) the contact area again remains constant. In the third region (3) the contact area decreases either uniformly marking the peeling mode of debonding (A) or in steps as in (B) marking the column collapse mode of failure.

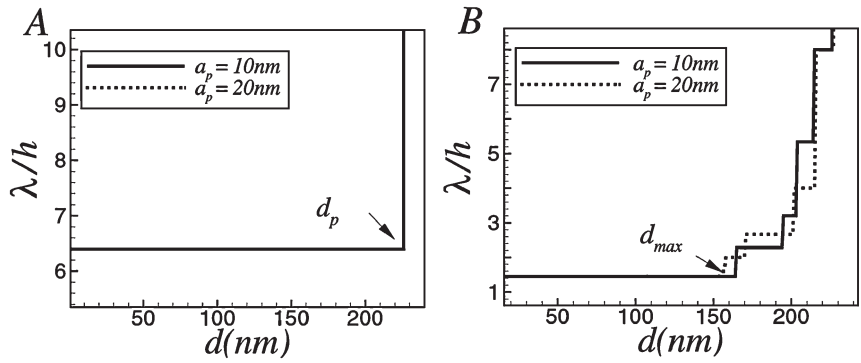

FIGURE 8 Lengthscales of the structures starting from intimate contact for a film as in Figure 7 and a step contactor of wavelength (A) $\lambda_p = 6.4\,h$ and (B) $\lambda_p = 1.45\,h$. In (A) $\lambda \sim \lambda_p$ up to snap-off and in (B) $\lambda \sim \lambda_p$ up to d_{max} after which it increases.

of roughness (Figs. 7(A) and (B)). The reasons for these differences between different contactor geometries are as follows. The presence of a sharp discontinuity causes a marked difference in the attractive forces present between two adjacent domains. Thus, the film does not cling to the sidewalls of a protrusion even if the contactor is pressed moderately. The initial contact area formed at d_c during further approach thus does not change as seen from Figure 7(A) and (B). So there is effectively no hysteresis present in the contact area for such cases. The contact area also remains unaffected by the amplitude of the profile of the contactor but depends only on the protruded area available for contact, which remain the same both for higher and smaller amplitude roughness.

The wavelength of the films obtained for the step contactors are shown in Figures 8(A) and (B). For higher periodicity of the contactor surface ($\lambda_p = 6.4\,h$) where peeling mode of failure is present, the spacing between the columns formed is the same as that of the contactor features until snap-off (Fig. 8(A)). While for small periodicities, for example, $\lambda_p = 1.45\,h$, the dominant wavelength begins to increase with separation distance once d_{max} is reached because of the presence of the column collapse mode of debonding (Fig. 8(B)).

FORCES, CHARACTERISTIC DISTANCES AND WORK DONE

In this section we focus on the force-displacement graphs that arise during debonding. Figure 9 depicts the force per unit area (F) that is

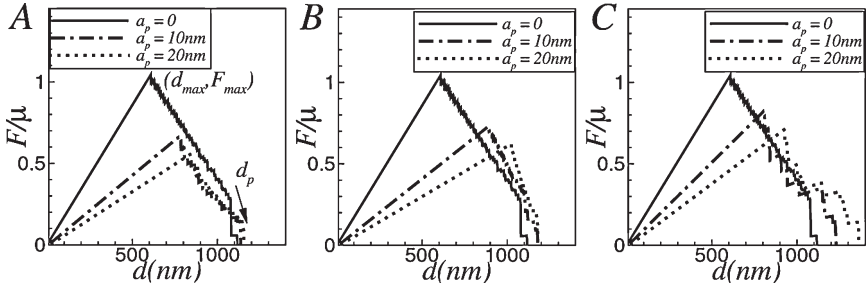

FIGURE 9 Variation of average stresses at the surface of a film of $h = 5.0\,\mu$m, $\mu = 0.1\,$MPa, $A = 10^{-20}$J when withdrawn from d_c (~10.67 nm) at a step-size of 1 nm. The sinusoidal contactor under consideration has a wavelength of 6.4 h, 3.2 h, and 1.45 h in (A), (B), and (C), respectively.

exerted on the sinusoidal contactor to hold the film in equilibrium at a given separation distance. This is in turn equal to the average stress developed in the film ($F = 1/L_1 \int_0^{L_1} \sigma_{22}(x_1, 0)dx_1$). The general force diagram shows that during the constant contact area branch when the columns remain pinned and elongate with the contactor, the average stresses in the film increases linearly with the separation distance. At d_{max} the force reaches a maximum and thereafter the average stresses at the film surface decreases. Figures 9(A), (B), and (C) show the non-dimensional force curve for a film of $h = 5\,\mu$m, $\mu = 0.1\,$MPa and $A = 10^{-20}$J and sinusoidal contactors with periodicities greater, similar or less ($\lambda_p = 6.4\,$h, $\lambda_p = 3.2\,$h, $\lambda_p = 1.45\,$h) than the natural wavelength of the instability for a smooth contactor ($\lambda = 3\,$h). Each of the figures shows the three cases for which the amplitude of the contactor is 0 (smooth), 10 nm or 20 nm. It is evident from the figures that with increase in the amplitude of roughness, the maximum force decreases for all contactors. The reason is the reduced contact area formed for larger amplitude rough surfaces. The initiation of peeling mode or column collapse mode marked by d_{max} is delayed by the introduction of roughness, which causes a more persistent pinning mode. This implies that introduction of roughness helps the film to remain trapped in a local energy minimum at increased separation distances. An increase in the amplitude of roughness similarly also increases the snap-off or debonding distance where the contact vanishes (Fig. 9). This reduction in the maximum force and increase in the snap-off distance with increased amplitude has indeed been observed in experiments on debonding from rough surfaces [13].

The simulations were carried out over a realistic range of parameters: $A = 10^{-20}$J, $\mu = 0.1$MPa, $h \sim 0.1$–$10\,\mu$m, $\alpha_{initial}(d \sim d_c)$ or $\alpha_{initial}$ $(d \sim 1\,nm)$, $s \sim 1 - 2$ nm, $\varepsilon = 0 - 0.01$, $a_p \sim 0$, 10 nm, 20 nm and $\lambda_p \sim 6.4$ h, 3.2 h, 1.45 h. The quantitative scalings obtained for the maximum pull-off force F_{max}, separation distance at the maximum pull-off force, d_{max}, snap-off distance d_p and the work of debonding, W (the area under the force-separation curve) are as follows:

$$\frac{F_{\max} h}{\mu d_e} \sim C_F \left(\frac{\Delta G h}{\mu d_e^2} \right)^{\delta} \tag{7}$$

$$\frac{d_{\max}}{d_e} \sim C_{d_m} \left(\frac{\Delta G h}{\mu d_e^2} \right)^{q} \tag{8}$$

$$\frac{d_p}{d_e} \sim C_{d_p} \left(\frac{\Delta G h}{\mu d_e^2} \right)^{p} \tag{9}$$

$$\frac{W}{\Delta G} \sim C_W \left(\frac{\Delta G h}{\mu d_e^2} \right)^{n} \tag{10}$$

where $\Delta G h / \mu {d_e}^2$ is compliance of the film defined as the ratio of the adhesive stiffness $(\Delta G / {d_e}^2)$ to the elastic stiffness (μ / h) of the film. Figure 10 shows the effect of amplitude of roughness on the above scalings when λ_p of the contactor is 1.45 h and the step-size of withdrawal, $s = 2$ nm. Figure 10(A) shows that although increase in roughness (a_p) does not affect the scaling for rough surfaces, it decreases the maximum force considerably as observed from Figure 9. The increase in amplitude of roughness ($a_p = 0$; flat contactor) to $a_p = 20$ nm also increases d_{max} and the snap-off distance d_p (Figs. 10(B) and (C)), although the slopes of the curves (q and p) decrease with a_p. It is evident that increased roughness increases the snap-off distance and decreases the maximum force to such an extent that the work-done for a flat contactor is always higher than for a rough contactor, as is evident from Figure 10(D).

Figure 11 shows that decrease in the periodicity of roughness (decrease in λ_p from 6.4 h to 1.45 h) increases the maximum pull-off force and δ slightly. As discussed earlier, there is greater tendency for intermittent column collapse with larger number of slender columns as periodicity decreases. With decreased periodicity, d_{max} and snap-off distance (Figs. 11(B) and (C) respectively) increase. The work of adhesion also increases with decrease in λ_p as evident from Figure 11(D).

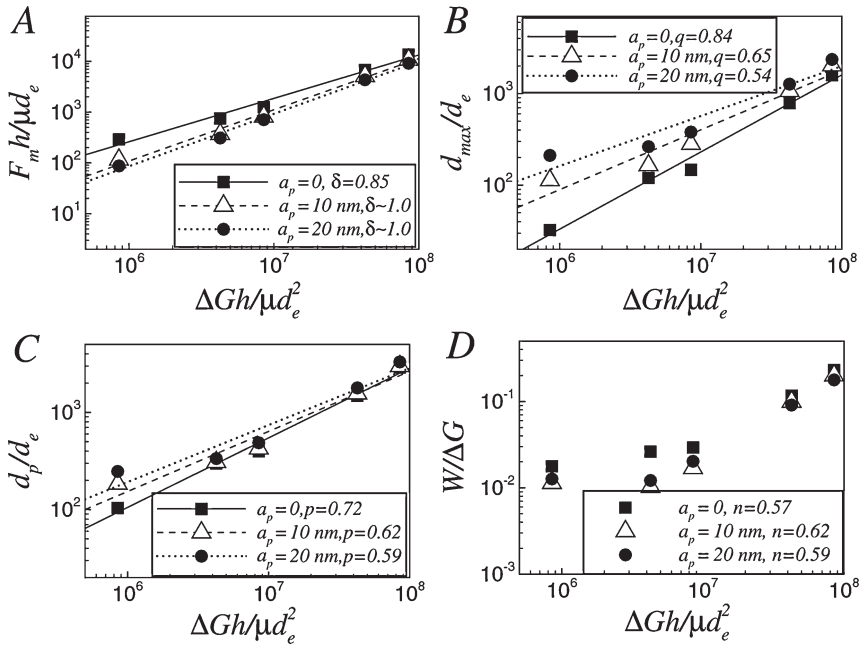

FIGURE 10 The effect of amplitude of roughness of the sinusoidal contactor of $\lambda_p = 1.45$ h, on (A) the maximum force (F_m), (B) the distance characteristic of the maximum force (d_{max}), (C) the snap-off distance (d_p), and (D) the area under the force curve or the work of adhesion (W) for films with $A = 10^{-20}$J, $\mu = 0.1$ MPa and $h = 0.1$–$10\,\mu$m, when withdrawn at a step size of 2 nm.

Figure 12 depicts the force-displacement curves for a film with $h = 5.0\,\mu$m, $\mu = 0.1$ MPa, $A = 10^{-20}$J when debonding phase is initiated from intimate contact for the contactors with $\lambda_p = 6.4$ h, 3.2 h, and 1.45 h, as shown in Figures (A), (B) and (C) respectively. If comparisons are made with the case of debonding phase starting from d_c (Fig. 9), it is evident that for all λ_p, the maximum force increases with a simultaneous shortening of the pinned phase. The latter is reflected in a decrease in d_{max}. The snap-off distance, however, remains the same irrespective of the way in which debonding is initiated—either starting either from d_c (Fig. 9) or from a more intimate contact (Fig. 12). Figure 13 brings out the comparison in the scalings for the two cases in a very comprehensive way. Figure 13(A) shows that the peak force always increases with increased initial area of contact for any contactor roughness. However, for a smooth contactor, the force increases more drastically by about 100% and the scaling

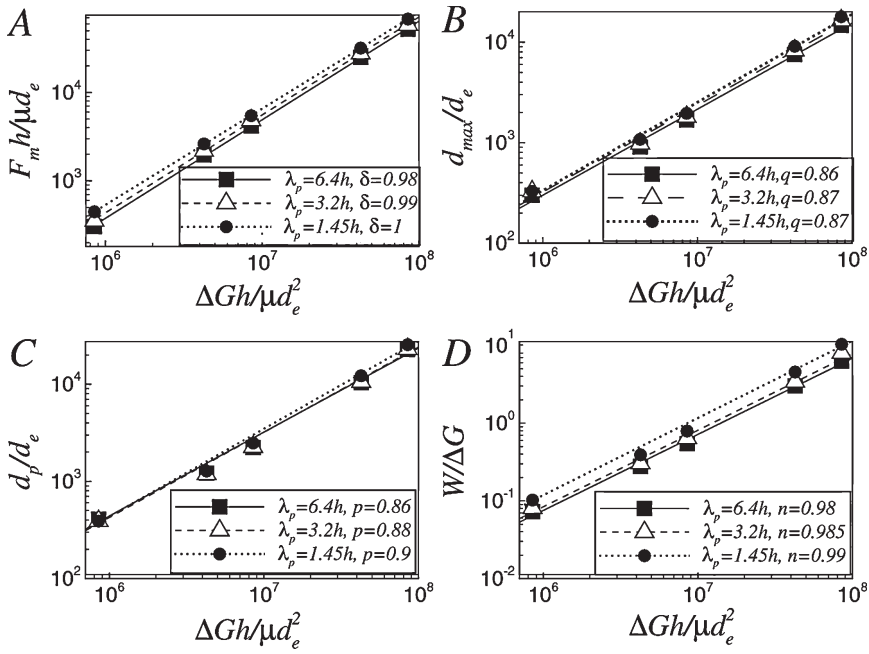

FIGURE 11 The effect of roughness lengthscale of the sinusoidal contactor of $a_p = 20\,\text{nm}$, on (A) the maximum force (F_m), (B) the distance characteristic of the maximum force (d_{max}), (C) the snap-off distance (d_p), and (D) the area under the force curve or the work of adhesion (W) for the range of parameters same as in Figure 10, when withdrawn at a step-size of 1 nm.

δ increases from 0.85 to 0.91. The change is, however, not as drastic for rough contactors, where the maximum force is only slightly changed depending on the initial contact area. The scaling for d_{max} is shown in Figure 13(B), which indicates that for smooth contactors, q changes rather drastically from 0.84 to 0.4. However, the change is less for rough contactors, $a_p = 10$ and 20 nm. The scaling for the snap-off distance is not affected by the initial contact area, $\alpha_{initial}$ (Figure 13(C)). Finally, the work done as well as its scaling exponent, n increases with more intimate contact as evident from Figure 13(D). Thus, from both Figures 12 and 13 it can be concluded that the effects of initial contact conditions are more pronounced when the contactor roughness is less.

The effect of step-size of withdrawal is shown in Figure 14 for a film with $h = 1.0\,\mu\text{m}$, $\mu = 0.1\,\text{MPa}$, $A = 10^{-20}\text{J}$, interacting with a sinusoidal contactor of amplitude, $a_p = 10\,\text{nm}$ and wavelength of 6.4 h, 3.2 h, and 1.45 h, as shown in Figures (A), (B), and (C), respectively. Increase in the step-size helps the film to escape the local energy

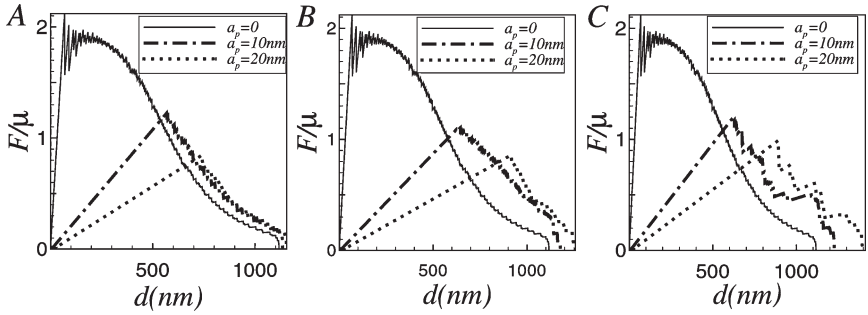

FIGURE 12 Variation of average normal stress at the surface of a film when withdrawn from intimate contact. The other conditions remain same as in Figure 9.

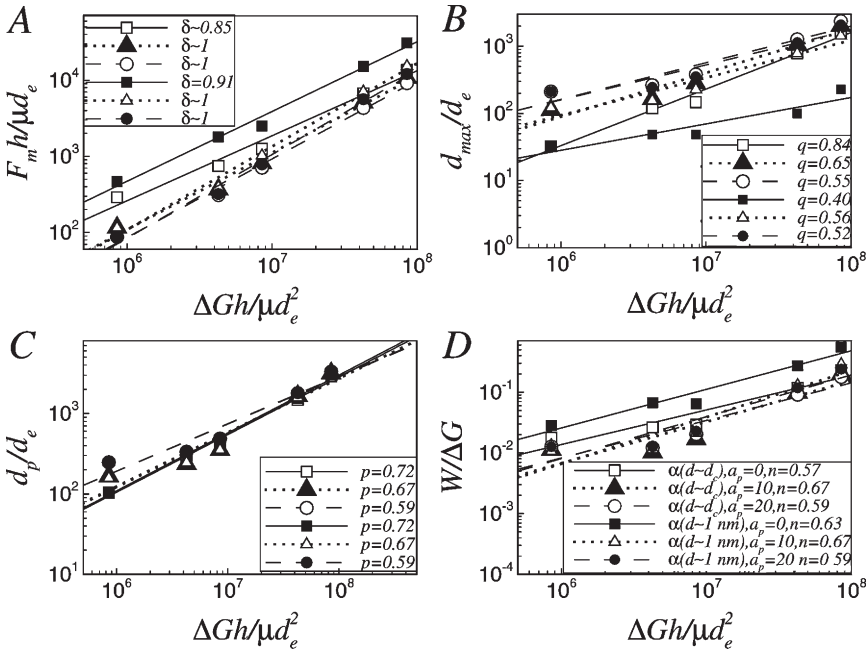

FIGURE 13 The effect of initial contact area on: (A) the maximum force, F_m, (B) the distance characteristic of the maximum force, d_{max}, (C) the snap-off distance, d_p, and (D) the area under the force curve or the work of adhesion, W. The wavelength of the sinusoidal contactor surface is $\lambda_p = 1.45\,\mathrm{h}$ and the step-size of withdrawl is 2 nm. Parameters are same as in Figure 10. Symbols in all the figures have the same meaning as shown in figure (D).

minimum in which it is trapped and transit to another nearby deeper energy minimum. This facilitates the transition from pinning to the peeling or column collapse mode of failure. This is evident from Figure 14, which shows that the peak force, the snap-off distance, the area under the force-displacement curve (work done) and d_{max} all decrease on the increase of step-size. Further, Figure 15 shows that although an increase in the step-size does not change the scaling for the maximum force very much, it decreases the exponents for the scalings of d_{max}, d_p, and W considerably.

The effect of introduction of noise can be seen from Figure 16, for the same case as discussed in Figure 14 when the sinusoidal contactor is withdrawn at a step-size of 1 nm. It is evident from the figure that whatever be the wavelength of the contactor, the introduction of noise has similar effects as that of increased step-size in finding the deeper energy minima. Hence F_{max}, d_{max}, d_p, and work of adhesion W are seen to decrease with increasing noise. Figure 17 shows that all the exponents, δ, q, p, and n can reduce substantially on introduction of noise for the case of a sinusoidal contactor.

Figure 18 depicts the force diagram for step profile contactors when debonding starts from critical separation distance. It is evident from the figure that there are little differences in F_{max}, d_{max}, and d_p with the amplitude and periodicity of the sharp cornered step-profile contactors ($a_p = 0$, 10 nm, 20 nm; $\lambda_p = 6.4$ h, $\lambda_p = 3.2$ h, $\lambda_p = 1.45$ h). On the other hand, when the simulations are carried out starting from a more intimate contact (refer to Fig. 19), there is a marked difference in the force curves (including the maximum force F_{max} and d_{max}) obtained for flat contactors and the step-profile contactors ($a_p = 10$ nm, 20 nm).

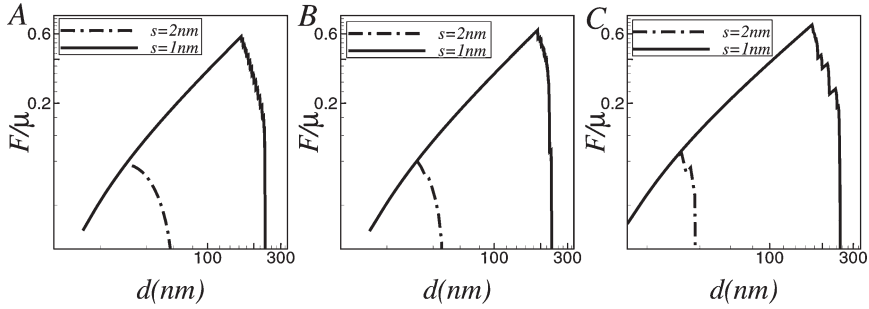

FIGURE 14 Average normal stress at the surface of a film of $h = 1.0\,\mu$m, $\mu = 0.1$ MPa, $A = 10^{-20}$ J when it is withdrawn at different step-sizes ($s = 1$ nm and 2 nm). The contactors have amplitude of 10 nm and wavelengths of 6.4 h, 3.2 h, and 1.45 h in (A), (B), and (C) respectively.

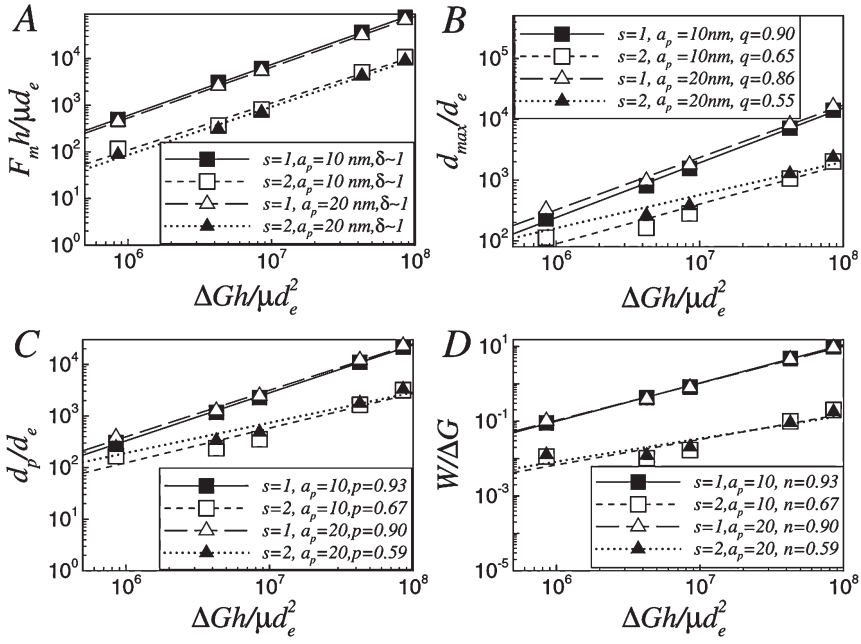

FIGURE 15 The effect of step-size on (A) the maximum force, F_m, (B) the distance characteristic of the maximum force, d_{max}, (C) the snap-off distance, d_p, and (D) the area under the force curve or the work of adhesion, W. Parameters are same as in Figure 10.

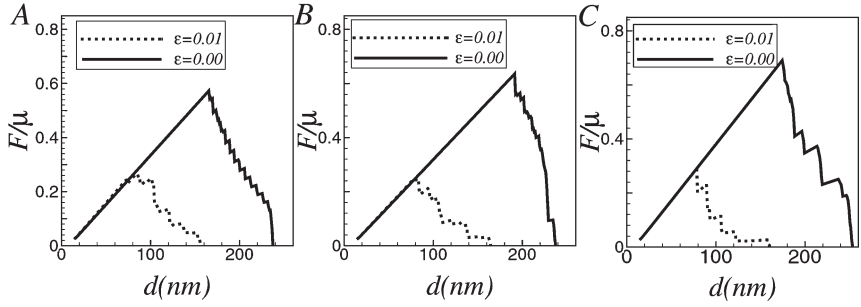

FIGURE 16 Effect of noise on the average normal stress with $h = 1.0\,\mu$m, $\mu = 0.1$ MPa, $A = 10^{-20}$J and step-size of 1 nm. The contactor has an amplitude of 10 nm and a wavelength of 6.4 h, 3.2 h, and 1.45 h in (A), (B), and (C), respectively.

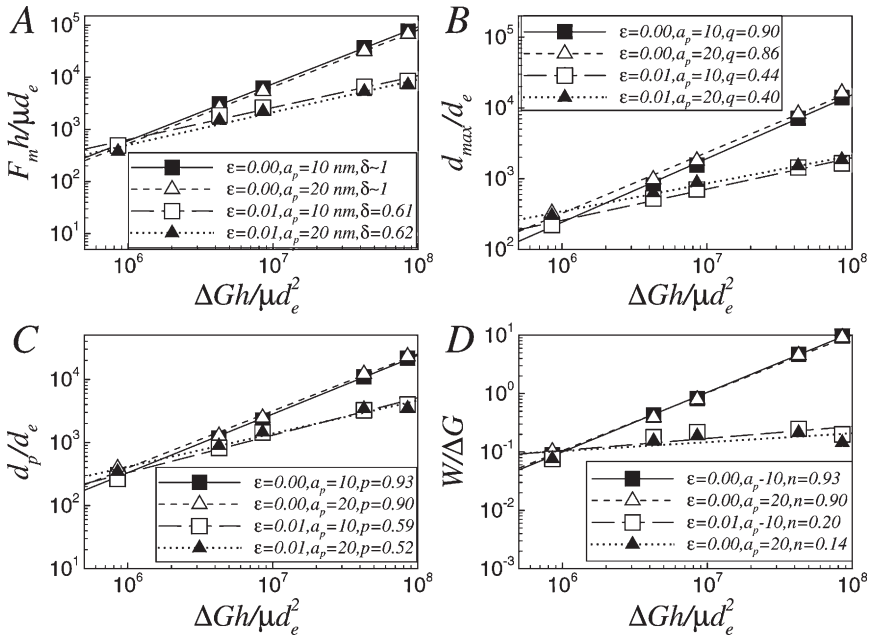

FIGURE 17 The effect of introduction of noise on (A) the maximum force, F_m, (B) the distance characteristic of the maximum force, d_{max}, (C) the snap-off distance, d_p, and (D) the area under the force curve or the work of adhesion, W. A sinusoidal contactor of wavelength $\lambda_p = 1.45\,\mathrm{h}$ is being withdrawn with a step-size of 1 nm. Parameters are same as in Figure 10.

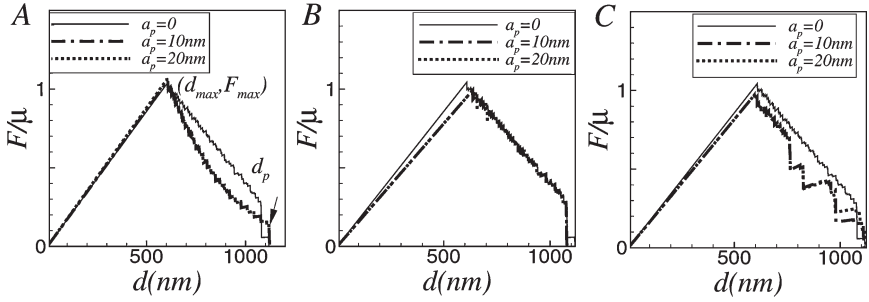

FIGURE 18 Variation of average normal stress at the surface of a film of $h = 1.0\,\mu\mathrm{m}$, $\mu = 0.1\,\mathrm{MPa}$, $A = 10^{-20}\mathrm{J}$ when the step-size of withdrawal is 1 nm. The contactors have step profiles with wavelengths 6.4 h, 3.2 h, and 1.45 h in (A), (B), and (C), respectively.

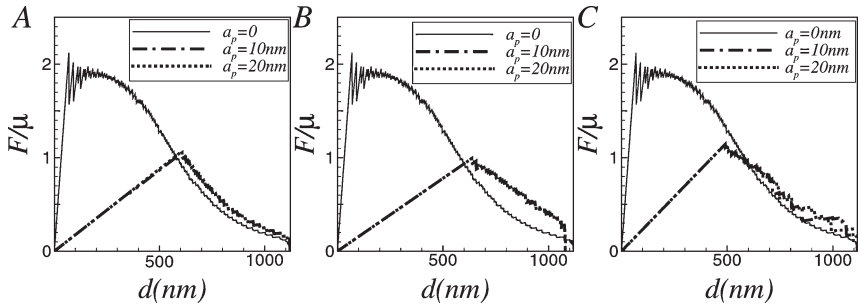

FIGURE 19 Variation of average stress at the surface of a film when withdrawn from intimate contact ($d_{eff} \sim 1$ nm). The other conditions remain same as in Figure 18.

There is a marked absence of hysteresis in step-profiled contactors (as observed from Fig. 7), but substantial hysteresis associated with smooth contactors (results not shown) and sine-wave contactors (Fig. 3). The whole process of debonding remains rather unaffected by the amplitude of the step-profiled contactor at moderate amplitudes. This is because of the constant contact area available for such film–contactor systems regardless of the amplitude, as discussed earlier. Thus, the force-displacement behavior and the quantities (F_{max}, d_{max}, d_p) obtained in both cases of debonding either from d_c (Fig. 18) or intimate contact (Fig. 19) remain unaffected by the amplitude of roughness. The introduction of noise and higher step-size for the step profiles has similar effects as in the case of sinusoidal contactors. As discussed earlier, both of these factors decrease F_{max}, d_{max}, d_p, and W_{max}. The scalings for these quantities are almost similar to those obtained from flat contactors in the case of withdrawal initiated from d_c since there is no significant influence of initial contact area.

USE OF PATTERNED CONTACTORS AS TEMPLATES

With a patterned contactor surface, the instabilities can be tailored to occur at the protruded areas of the contactor and in this way the patterned contactors can be used as templates for patterning of soft elastic films. In this section, we briefly address the issue of 3-D morphologies of soft elastic films under the influence of patterned contactors. For this purpose a 3-D model has been considered where the profile of the contactor plate is same as that shown in Figure 1 throughout the finite length of the film L_3 (distance of the film considered along x_3 direction and perpendicular to the x_1–x_2 plane shown

in Fig. 1) and the displacement field of the film along the direction normal to the surface of the film is now given by

$$\begin{aligned} v_2^{\mathrm{f}}(\mathrm{x}_1, 0, \mathrm{x}_3) = \sum_{m=0}^{M-1}\sum_{n=0}^{N-1} & v_{cc}(m,n)\cos(k_m x_1)\cos(k_n x_3) \\ & + v_{cs}(m,n)\cos(k_m x_1)\sin(k_n x_3) \\ & + v_{sc}(m,n)\sin(k_m x_1)\cos(k_n x_3) \\ & + v_{ss}(m,n)\sin(k_m x_1)\sin(k_n x_3) \end{aligned}$$

where v_{cc}, v_{cs}, v_{sc}, v_{ss} are the Fourier coefficients and $k_l = \sqrt{(k_m^2 + k_n^2)}$ is the wave-number corresponding to m and n mode of deformation where $k_m = 2\pi m/L_1$ and $k_n = 2\pi n/L_3$. The energy of the film in terms of the 3-D Fourier coefficients can be obtained along the same lines as discussed in the first section and is not repeated here.

Following the same procedure of energy minimization by conjugate gradient method (which now involves more numerically intensive simulations) one arrives at the morphologies presented in Figures 20 and 21 at the critical separation distance for contactors with step-change and sinusoidal profiles, respectively. Figure 20(A) shows the morphology of the film when it is in contact proximity of a flat contactor. The patterns obtained are labyrinth like, where the darker regions are the regions of contact. The dominant wavelength of the features formed is close to 3 h as expected from linear stability analysis [21–23]. When the central portion of the contactor has a large step-like protruded area, the film comes in contact with the central zone of the contactor as shown in Figure 20(B) with segregated regions of contact in the form of islands (denoted by the darker regions). When the wavelength of the pattern decreases (5 steps in $L_1 = 32$ h), the area of each step decreases, but the film still does not cover the entire protruded area. The contact regions remain fragmented as shown in Figure 20(C). It is only when the periodicity of the patterned contactor is close to the natural wavelength of the instability ($\lambda \sim 3$ h) that one obtains near ideal templating as shown in Figures 20(D) and (E). Further increase in the number of steps (per unit length) leads to the formation of partially disintegrated columns along their length as shown in Figure 20(F). Figure 21 shows a similar scenario with sinusoidal contactors. When the periodicity of the patterned sinusoidal contactor is high ($\lambda_p = 16$ h), there is formation of finger like structures along the edges of the columns as seen from Figure 21(A). With decrease in $\lambda_p (= 8$ h) there is however ideal templating, where the columns mimic the structure of the patterned contactor, the crests of the contactor comes in total contact with the crests of the patterns formed at the film

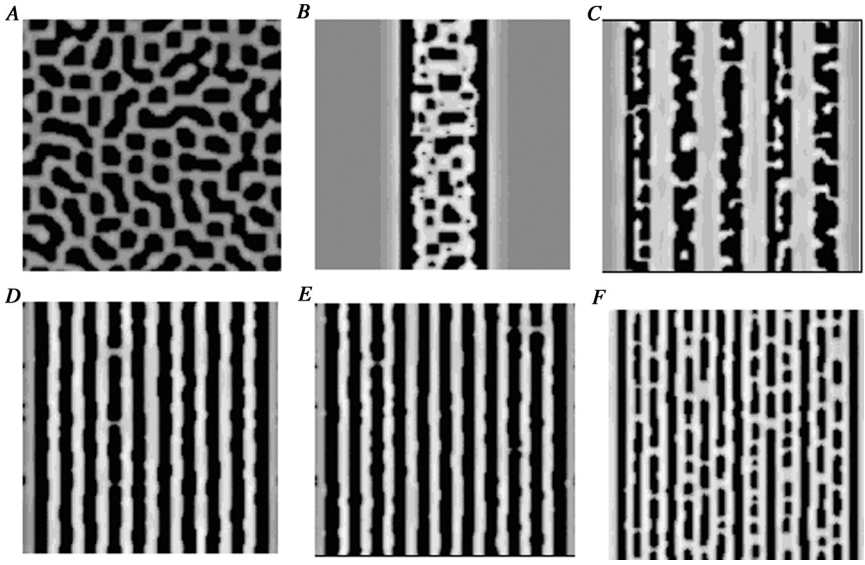

FIGURE 20 The 2-D contour plots showing the morphologies of a film with $h = 10.0\,\mu\text{m}$, $\mu = 0.1\,\text{MPa}$, $A = 10^{-20}\,\text{J}$ at $d_c(\sim 12\,\text{nm})$ under the influence of step profiled contactors with number of steps, $N = 0$, 1, 5, 10, 11, 15 for (A), (B), (C), (D), (E), and (F), respectively. Each figure represents an area of $320\,\mu\text{m} \times 320\,\mu\text{m}$. The darker regions represent regions of contact. For the smooth contactor, labyrinth type of pattern as in (A) is obtained, whereas for (D) and (E), ideal patterning of the film surface is observed.

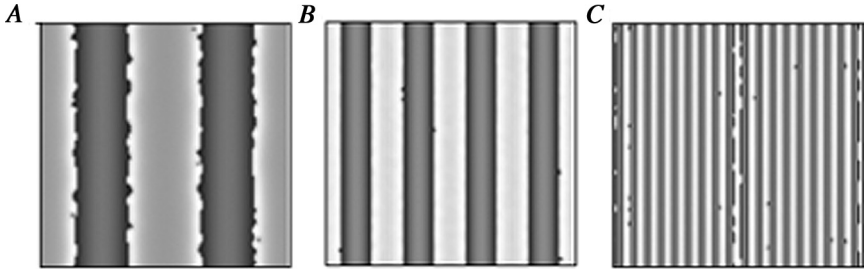

FIGURE 21 The 2-D contour plots showing the morphologies of the film (same as in Figure 21) at d_c now under the influence of a sinusoidal contactor with wavelength $\lambda_p = 16\,\text{h}$ (Fig. A), 8 h (Fig. B) and 1.8 h (Fig. C), respectively. Fingering at the edges of the columns is observed in (A), conditions in (C) give rise to disintegrated column formation and (B) represents the case of ideal templating.

surface. With further decrease in periodicity $\lambda_p (= 1.8\,\mathrm{h})$, there are again finger like structures hampering the formation of ideally templated patterns as shown in Figure 21(C).

CONCLUSIONS

In this paper we have simulated the influence of a patterned rough contactor on the adhesion-debonding cycle of an elastic film. The main results are summarized in the following section.

(1) When the effective separation distance between the protruded area of the contactor and the surface of the film declines to below a critical distance, columns form spontaneously at the surface of the film and adhere only with these projected zones of the contactor.
(2) During withdrawal phase, there appear two distinct phases. The first phase is the pinning zone where the film surface remains *pinned* to the rough contactor and elongates with the contactor without any change in the contact area. Here the average stress increases linearly with the separation distance. In the second phase starting from the peak force F_{max}, sideways peeling of contact zones relieves the average stress. When the wavelength of the patterned contactor is high ($\gg 3\,\mathrm{h}$), the decrease in the contact area upon withdrawal is uniform and the mode of failure is termed as the *peeling mode*. In contrast, when the wavelength of the patterned contactor is low, the contact area decreases in a step-wise fashion due to the intermittent collapse of slender columns.
(3) Increase in the amplitude of roughness is found to decrease the maximum force required for debonding and increase the snap-off distance. The combined effect results in a decrease of work done for debonding from a rough surface. These changes are indeed observed experimentally in debonding of PSA from rough surfaces [13].
(4) The effect of initial contact conditions is seen to have less influence for a rough contactor as compared to a smooth contactor. In the latter case, adhesion-debonding hysteresis of force and morphology is also more pronounced.
(5) Introduction of increased noise and step-size reduce the maximum force, distance at which the peak force occurs, the final snap-off distance and the work done in debonding. These effects are similar to the case of a flat contactor.
(6) Our preliminary 3-D simulations indicate that a patterned contactor can be used as a template for the creation of desired patterns

in a soft elastic film. Conditions for ideal templating require that the contactor periodicity be in the vicinity of the natural length scale ($\lambda \sim 3\,h$) of the surface instability with a smooth contactor.

REFERENCES

[1] Lin, Y. Y., Hui, C.-Y., and Conway, H. D., *J. Polymer Sci. Part B: Polymer Phys*. **38**, 2769–2784 (2000).
[2] Creton, C., Hooker, J., and Shull, K. R., *Langmuir* **17**, 4948–4954 (2001).
[3] Crosby, A. J., Shull, K. R., Lakrout, H., and Creton, C., *J. Appl. Phys*. **88**, 2956–2966 (2000).
[4] Wan, K. T., *J. Adhesion* **75**, 369–380 (2001).
[5] Gent, A. N. and Petrich, R. P., *Proc. Roy. Soc. London. A* **310**, 433–448 (1969).
[6] Gay, C. and Leibler, L., *Phys. Rev. Lett*. **82**, 936–939 (1999).
[7] Chikina, I. and Gay, C., *Phys. Rev. Lett*. **85**, 4546–4549 (2000).
[8] Brown, K., Hooker, J. C., and Creton, C., *Macromol. Materials Engg*. **287**, 163–179 (2002).
[9] Greenwood, J. A. and Williamson, J. B. P., *Proc. R. Soc. London Ser. A* **A295**, 300 (1996).
[10] Johnson, K. L., *Proc. R. Soc. London Ser. A* **453**, 163–179 (1997).
[11] Hui, C.-Y., Lin, Y. Y., and Baney. J. M., *J. Polymer Sci. Part B: Polymer Phys*. **38**, 1485–1495 (2000).
[12] Hui, C.-Y., Lin, Y. Y., and Creton, C., *J. Polymer Sci. Part B: Polymer Phys.* **40**, 545–561 (2002).
[13] Chiche, A., Pareige, P., and Creton, C., *C. R. Acad. Sci. IV-Phys*. **1**, 1197–1204 (2000).
[14] Sarkar, J., Shenoy, V., and Sharma, A., *Phys. Rev. Lett*. **93**, 018302 (4) (2004).
[15] Sarkar, J., Sharma, A., and Shenoy, V., *Langmuir*, **21**, 1457–1469 (2005).
[16] Mönch, W. and Herminghaus, S., *Euro. Lett*. **53**, 525–531 (2001).
[17] Ghatak, A., Chaudhury, M. K., Shenoy, V., and Sharma, A., *Phys. Rev. Lett.* **85**, 4329–4332 (2000).
[18] Ghatak, A. and Chaudhury, M. K., *Langmuir* **19**, 2621–2631 (2003).
[19] Shull, K. R., Flanigan, C. M., and Crosby, A. J., *Phys. Rev. Lett*. **84**, 3057–3060 (2000).
[20] Webber, R. E., Shull, K. R., Roos, A., and Creton, C., *Phys. Rev. E* **68**, 021805 (11) (2003).
[21] Shenoy, V. and Sharma, A., *Phys. Rev. Lett*. **86**, 119–122 (2001).
[22] Shenoy, V. and Sharma, A., *J. Mech. Phys. Solids* **50**, 1155–1173 (2002).
[23] Sarkar, J., Shenoy, V., and Sharma, A., *Phys. Rev. E* **67**, 031607 (11) (2003).
[24] Ru, C. Q., *J. Appl. Mech-T Asme*. **69**, 97–103 (2002).
[25] Asaro, R. J. and Tiller, W. A., *Metall. Trans*. **3**, 1789–1796 (1972).
[26] Grinfield, M., *J. Nonlinear Sci*. **3**, 35–83 (1993).
[27] Srolovitz, D. *Acta Metall*. **37**, 621–625 (1989).
[28] Ramirez, J. C., *Int. J. Solids Struct*. **25**, 579–589 (1989).
[29] Schäffer, E., Thurn-Albrecht, T., Russel, T. P., and Steiner, U., *Nature* **403**, 874–877 (2000).
[30] Herminghaus, S., Jacobs, K., Mecke, K., Bischof, J., Fery, A., Ibn-Elhaj, M., and Schlagowski, S., *Science* **282**, 916–919 (1998).
[31] Sharma, A. and Khanna, R., *Phys. Rev. Lett*. **81**, 3463–3466 (1998).
[32] Reiter, G., Khanna, R., and Sharma, A., *Phys. Rev. Lett*. **84**, 1432–1435 (2000).